CHEMISTRY
A European Journal

Accepted Article

Title: Dynamic disorder restriction of methyl-ammonium (MA) groups in chloride-doped MAPbBr3 hybrid perovskites: a neutron powder diffraction study

Authors: Carlos Alberto Lopez, Maria Consuelo Alvarez-Galvan, Maria Victoria Martinez-Huerta, Maria Teresa Fernandez-Diaz, and Jose Antonio Alonso

WILEY-VCH

FULL PAPER

Dynamic disorder restriction of methyl-ammonium (MA) groups in chloride-doped MAPbBr$_3$ hybrid perovskites: a neutron powder diffraction study

Carlos Alberto López,*[a-b] María Consuelo Álvarez-Galván,[c] María Victoria Martínez-Huerta,[c] María Teresa Fernández-Díaz[d] and José Antonio Alonso*[a]

Abstract: The hybrid methyl-ammonium (MA) lead halide MAPbX$_3$ perovskites present an appealing optoelectronic behavior with applications in high-efficiency solar cells. The orientation of the organic MA units may play an important role in the properties, given the degrees of freedom for internal motion of MA groups within the PbX$_6$ network. The present neutron powder diffraction study reveals the dynamic features of the MA units in the hybrid-perovskite series MAPb(Br$_{1-x}$Cl$_x$)$_3$, with x = 0, 0.33, 0.5, 0.67 and 1. From difference Fourier maps, the H and C/N positions were located within the PbX$_6$ lattice; the refinement of the crystal structures unveiled the MA conformations. Three different orientations were found to exist as a function of the chlorine content (x) and, therefore, of the cubic unit-cell size. These conformations are stabilized by H-bond interactions with the halide ions, and were found to agree with those reported from theoretical calculations.

Introduction

Methyl-ammonium (MA) lead halide perovskites CH$_3$NH$_3$PbX$_3$ (X = I, Br, Cl), and their mixed-halide crystals have attracted wide interests in recent years due to their applications in optoelectronic devices.[1–6] While methylammonium lead iodide (MAPbI$_3$) remains the most widely studied perovskite due to its ability to absorb broadband light below its bandgap of 1.6 eV, the degradation in a humid atmosphere has remained a major obstacle for commercialization.[7] MAPbBr$_3$ is a promising alternative to MAPbI$_3$ with a large band-gap of 2.2 eV, which gives rise to a high open circuit voltage (Voc ≈ 1.2–1.5 V).[8] Their long exciton diffusion length (>1.2 μm) enables good charge transport in devices. In addition, MAPbBr$_3$ demonstrates higher stability towards air and moisture due to its stable cubic phase and low ionic mobility relative to the pseudocubic MAPbI$_3$.[9] MAPbCl$_3$

possesses a wide band gap of 3.11 eV and it is visibly transparent but sensitive to the ultraviolet (UV) region. It has been reported that the trap-state density, charge carrier concentration, mobility, and diffusion length of MAPbCl$_3$ are comparable with those of the best quality crystals of MAPbI$_3$ and MAPbBr$_3$.[10]

It is evident that the methyl-ammonium configuration plays an important role in the physical and optical properties and must be taken into account for the design of optoelectronic materials. The first evidences of MA rotations in lead halide perovskites were reported by Wasylishen et al. in 1985 from Nuclear Magnetic Resonance (NMR).[11] Later this MA rotation was evidenced from X-ray diffractions techniques,[12,13] and then Yamamuro et al. proposed three possible orientations: [111], [110] and [100] in the cubic system.[14] Although the MA orientation restrictions described for the low-symmetry phases observed at low temperatures (tetragonal - orthorhombic) are well known,[15–18] the delocalization in the cubic system still remains uncertain. Recently, many authors have studied the MA groups in the PbX$_6$ framework using theoretical and experimental tools. From experimental methods, the MA delocalization has been reported to happen in the [110] direction [19]; however, the three mentioned orientation possibilities have only been induced from theoretical methods.[20–22]

In the present work, we present for the first time experimental evidences of the preferred MA configurations in the compounds of the MAPb(Br$_{1-x}$Cl$_x$)$_3$ series. Neutron powder diffraction with non-deuterated samples was an essential tool to unveil the MA orientations and the effect of the chloride doping in MAPbBr$_3$ hybrid perovskite.

Results and Discussion

The initial crystallographic identification was performed from laboratory XRD. All the samples exhibit a high purity; only for MAPbCl$_3$ minor amounts of MACl were identified. Figure 1 shows the XRD patterns of the obtained samples in comparison with MAPbBr$_3$.[8] As shown, the diffraction lines exhibit a systematic shift at high 2θ values as x increases, evidencing the decrease of the unit-cell size due to chloride introduction into the crystalline network. All the patterns can be indexed in a cubic symmetry with space group $Pm\bar{3}m$. Previous reports for MAPbX$_3$ with X = Br or Cl also described these phases in this cubic space group at room temperature.[8,17–19,23] A recent temperature-dependent synchrotron XRD study was useful to identify different phase transitions depending on the Cl contents.[24] However, the

[a]   Dr. C.A. López,* Dr. J.A. Alonso*
      Instituto de Ciencia de Materiales de Madrid, CSIC.
      Cantoblanco 28049 Madrid, Spain.
      E-mail: ja.alonso@icmm.csic.es
[b]   Instituto de Investigaciones en Tecnología Química (INTEQUI),
      UNSL-CONICET and Fac. de Qca., Bqca. y Far., UNSL.
      Ejercito de los Andes 950, 5700, San Luis, Argentine.
[c]   Dra. C. Álvarez-Galván, Dra. M.V. Martínez-Huerta.
      Instituto de Catálisis y Petroleoquímica, CSIC.
      Cantoblanco 28049 Madrid, Spain.
[d]   Dra. M.T. Fernández-Díaz
      Institut Laue Langevin.
      38042 Grenoble Cedex, France.

FULL PAPER

crystallographic features obtained from x-ray techniques (either laboratory or synchrotron; powder or single crystal) for these hybrid compounds are sketchy.
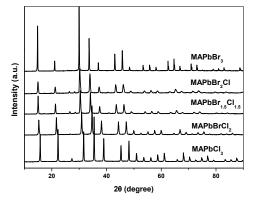

Figure 1. XRD patterns of synthesized samples in comparison with the parent MAPbBr$_3$ perovskite.

A neutron powder diffraction investigation was essential to obtain a more detailed description of these materials, in particular concerning the distribution of MA groups. As a first step, the initial refinements were performed using the Le Bail method in order to fit the instrumental parameters and refine the unit-cell parameters. Then, the structure of the covalent PbX$_6$ octahedral network was included in the model, where the lead atoms are placed at 1a (0,0,0) sites and bromine/chlorine atoms are statistically distributed at 3d (1/2,0,0) positions in the $Pm\bar{3}m$ space group. Next, difference Fourier maps (DFM) were obtained from the observed and calculated neutron powder diffraction data for each Br/Cl ratio.

From the same analysis in the parent compound of the series, MAPbBr$_3$, recently reported by us, it was shown that the MA groups are delocalized at room temperature along the [110] direction, involving six possible orientations.[8] However, the Cl-doped phases show different patterns with positive and negative nuclear densities, indicating that the delocalization of the MA units differ from those observed for the bromide phase. These differences in the nuclear density (in terms of scattering length density) will be analyzed individually.

The DFM for MAPbBr$_2$Cl is shown in Figures 2 a) and b). Here the positive and negative densities exactly match with those expected for the H$_3$C–NH$_3^+$ cations oriented along [111] directions. The negative scattering regions (represented in blue) are, of course, due to the negative scattering of protons. It is possible to deduce that the C/N and H atoms are placed at 8g (x,x,x) and 24m (x,x,z) Wyckoff positions, respectively. MAPbBr$_{1.5}$Cl$_{1.5}$ exhibits a peculiar negative distribution, as shown in Figure 2 c). There are four negative zones along the [001] directions, which suggests that the MA units are along this direction. However, a non-negligible density also appears along [111] directions, which is unrealistic. To discern this case, Figure 2 d) shows the positive surface

limited to 0.39 fm, which reveals that the C/N are indeed delocalized along the [100] directions. Hence, the C/N and H atoms are placed in this case at 6f ($x,0.5,0.5$) and 24l ($0.5,y,z$) Wyckoff positions, respectively.
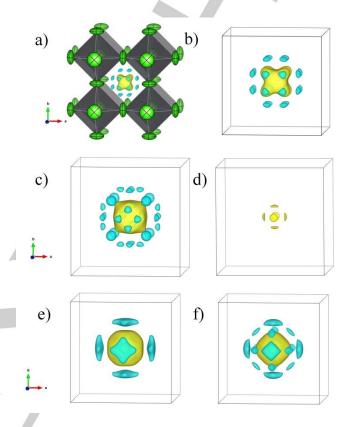

Figure 2. Selected DFM iso-surfaces of MAPb(Br$_{1-x}$Cl$_x$)$_3$, which illustrate the different orientations of the MA groups. a) and b) for MAPbBr$_2$Cl at δ = 0.15 fm. c) and d) for x = MAPbBr$_{1.5}$Cl$_{1.5}$ at δ = 0.13 and 0.39 fm, respectively. e) for MAPbBrCl$_2$ at δ = 0.1 and f) for MAPbBrCl$_3$ at δ = 0.1.

Following the same procedure for MAPbBrCl$_2$ and MAPbCl$_3$, see Figures 2 e) and f), it is possible to find that the MA groups are oriented along [100] directions, in the same way as MAPbBr$_{1.5}$Cl$_{1.5}$. Figure S1 (Supporting Information) illustrates the DFM for MAPbCl$_3$ in comparison with MAPbBr$_3$ reported previously by us.[8] From this result, a clear restriction in the MA delocalization is revealed, evolving from [110] to [111] and finally to [100] directions, while X is progressively enriched in Cl$^-$ anions.

Taking those results from the Fourier synthesis maps into account, the crystallographic models were completed with the MA configurations. Additionally, the MA displacement towards the -NH$_3$ group also was experimentally observed, as suggested from theoretical calculations and experimentally from single crystal neutron diffractions for MAPbBr$_3$.[22,25,26] The full refinement of the crystal structures yielded the NPD plots illustrated in Figure 3 for x = 0.33 and 1.00, and in Figure S2 for x = 0.50 and 0.67. The main crystallographic data are listed in Table 1 for x = 0.33 and 1.00 and in Table S1 for x = 0.50 and 0.67. Three different

FULL PAPER

combinations of C/N and H positions are observed in MAPb(Br$_{1-x}$Cl$_x$)$_3$ series, which allows for three possibilities for the MA delocalization in the PbX$_6$ framework. Figure 4 illustrates the variation of the unit-cell parameter with the Cl-doping, where an inflection point is observed in the perovskite with an equimolar amount of Br and Cl atoms. Analyzed from the point of view of the MA conformations, it is possible to observe that the unit-cell contraction upon Cl introduction keeps a constant slope when the MA direction is the same, (for x = 0.5, 0.67 and 1), whereas for x = 0 and 0.33, where the MA conformation is different, the unit-cell parameter falls apart from this slope.

From these observations, it underlays that the contraction of the PbX$_6$ framework upon Cl introduction limits the degree of freedom of the MA units, or it is closely related to the orientation of the organic group. This reduction in size was exhaustively studied across the reported phase transitions below room temperature (cubic – tetragonal – orthorhombic),[8,21,22,24,27]; however, this behavior is original if the same crystal system is maintained, as found in the CH$_3$NH$_3$Pb(Br$_{1-x}$Cl$_x$)$_3$ series at RT.

A singular case was found in the parent MAPbBr$_3$ described from NPD and SXRD data,[8] where the MA units are delocalized along [110] at RT; the reduction in size driven by cooling the sample down to 240 K, still described in the cubic $Pm\bar{3}m$ s.g., forced the MA units to delocalize along the [100] directions.[8]

This nice example shows that the reduction in size of the PbX$_6$ network, either by a decrease of the temperature or by chemical doping, leads to an orientation evolution of the organic group.

Table 1. Crystallographic parameters for MAPb(Br$_{1-x}$Cl$_x$)$_3$ with x = 0.33 and 1 phases refined in the cubic $Pm\bar{3}m$ space group from NPD data. The parameters for x= 0.5 and x= 0.67 are included in the SI.

a) MAPbBr$_2$Cl, a = 5.8454(8) Å

Atom	Wyckoff site	x	y	z	Uiso*/Ueq	Occ
Pb	1a	0	0	0	0.048(3)	1
Br	3d	0.5	0	0	0.096(5)	0.62(3)
Cl	3d	0.5	0	0	0.096(5)	0.38(3)
N1	8g	0.5809(5)	0.5809(5)	0.5809(5)	0.061(1)*	0.125
C2	8g	0.4378(5)	0.4378(5)	0.4378(5)	0.061(1)*	0.125
H11	24m	0.5839(6)	0.7363(9)	0.5839(6)	0.063*	0.125
H21	24m	0.4416(7)	0.2841(8)	0.4416(7)	0.063*	0.125
	U^{11}	U^{22}	U^{33}	U^{12}	U^{13}	U^{23}
Pb	0.048(3)	0.048(3)	0.048(3)	0.00000	0.00000	0.00000
N	0.028(5)	0.130(5)	0.130(5)	0.00000	0.00000	0.00000

Rp = 1.34%, Rwp = 1.71%, χ2= 1.14 and R$_{Bragg}$ = 10.80%

b) MAPbCl$_3$, a = 5.6813(5) Å

Atom	Wyckoff site	x	y	z	Uiso*/Ueq	Occ
Pb	1a	0	0	0	0.0239(4)	1
Cl	3d	0.5	0	0	0.0924(8)	1
N1	6f	0.5	0.5	0.6594(5)	0.039(1)*	0.16667
H11	24l	0.5	0.670(1)	0.720(2)	0.059(2)*	0.04167
H12	48n	0.6445(9)	0.4166(9)	0.720(2)	0.059(2)*	0.04167
C2	6f	0.5	0.5	0.4113(5)	0.039(1)*	0.16667
H21	24l	0.5	0.326(1)	0.351(2)	0.059(2)*	0.04167
H22	48n	0.354(1)	0.585(1)	0.351(2)	0.059(2)*	0.04167
	U^{11}	U^{22}	U^{33}	U^{12}	U^{13}	U^{23}
Pb	0.0239(4)	0.0239(4)	0.0239(4)	0.00000	0.00000	0.00000
Cl	0.0471(8)	0.1151(7)	0.1151(7)	0.00000	0.00000	0.00000

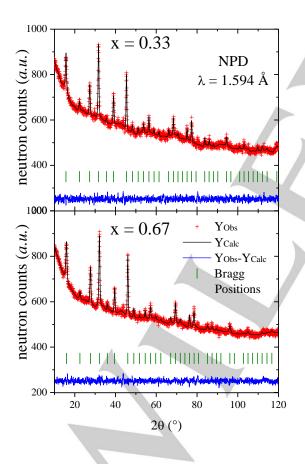Rp = 0.75%, Rwp = 0.94%, χ2= 1.23 and R$_{Bragg}$ = 6.36%

Figure 3. Observed (circles) calculated (back line) and difference (blue line) NPD profiles after the Rietveld refinement in a cubic unit cell for CH$_3$NH$_3$Pb(Br$_{1-x}$Cl$_x$)$_3$ with x = 0.33 (upper) and 1.00 (lower) at room temperature. The plots for x= 0.5 and 0.67 patterns are included in the SI.

It is important to remark the differences in the negative densities (H positions) observed between [111] and [001] orientations. While along the [111] direction, the three terminal H atoms of the

FULL PAPER

H$_3$C-NH$_3^+$ units are visualized at fixed positions (see Figures 2 b) and c)), along [100] the negative density seems to reveal four H atoms contained in the (100) plane (see Figures 2 c), e) and f)). This suggests that along the [100] orientation, the MA units can be rotated to four equivalent positions, so that each H points to each of the four halides in the edges of the perovskite unit cell, thus manifesting the importance of H⋯X hydrogen bonds. This bonded H is allocated in H11 site and the other two H of the amine group are allocated in H12 site. Similarly, the methyl groups are formed by C2, H21 and H22 atoms (Tables 1 and S1).
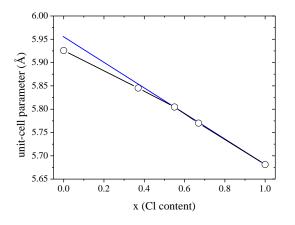
Figure 4. Unit-cell parameter as a function of x value in MAPb(Br$_{1-x}$Cl$_x$)$_3$. The error bars are much smaller than the experimental symbols.

The role of H⋯X interactions in the MA conformations is not unknown. Theoretical studies from density theory (DFT) indicate that the energy difference between the low index [100], [110] and [111] orientations of the MA units are similar, but with a subtle preference for the [100] orientation in the tetragonal MAPbI$_3$.[27] On the other hand, Shimamura *et al.* demonstrated from ab initio simulations that the H⋯X interactions in MAPbI$_3$ stabilized the [110] orientation instead of [111] and [100].[20] In contrast, Li *et al.* found that the more stable configurations are [111] and [100] for both MAPbI$_3$ and MAPbCl$_3$ perovskites.[26] Recently, Varadwaj *et al.* also reports these orientations ([111] and [100]) as the most energetically favorable.[22] In spite of these possibilities, there are few reports with experimental evidences concerning the MA orientation in cubic symmetry.[17–19] Out of these works, only Baikie *et al.*[19] report on the three structures for X = I, Br and Cl from X-ray and neutron diffraction data, where the MA units were refined in the [110] direction. Based on these previous theoretical studies, it is possible to achieve a detailed analysis of our crystal study. From the refined atomic positions for C, N and H it is possible to "deconvolute" the different MA orientations for both [111] and [100] directions and to compare the H⋯X interactions with those given by the theoretical studies.

Figure 5 a) illustrates a unique MA unit in the cubic unit cell for x = 0.33 (directed along [111] direction) where the H-C and H-N bonds interact with a unique halide ion (X = Cl$_{0.33}$Br$_{0.67}$) with distances of 2.921(5) and 3.088(5) Å, respectively. As mentioned

above, the MA unit is shifted, such that the (N)H⋯X distances are shorter than the (C)H⋯X ones, which is expected considering the greater electronegativity of N respect to C. DFT results for this configuration in MAPbBr$_3$ show that these distances are ≈2.44 and ≈3.47 Å for (N)H⋯X and (C)H⋯X, respectively, as reported by Varadwaj *et al.* from DFT calculations.[22] In spite of the different content of X= Br or Cl in these systems, both NPD and DFT results are in good agreement.

A similar analysis can be carried out for x = 0.5, 0.67 and 1, where the orientation is along [100]. As mentioned above, in this case the MA in each of the three [100] directions can be rotated in four positions, giving 12 possible conformations for the MA units. These conformations are also deduced from DFT calculations for bromine and chlorine phases.[22,26] Figures 5 b) and 5 c) illustrate a MA unit extract of the obtained C, N and H atomic positions for MAPbCl$_3$. As illustrated in Figures 5 b) and 5 c) with pale lines, there are two types of H-bond: normal (N1–H11⋯X) and bifurcated (N1–H12⋯X). In the same way, the methyl group shows the same interactions through H21 and H22 atoms. The obtained distances for x= 1 phase are 2.459(8) and 2.615(8) Å for N1–H11⋯X and N1–H12⋯X, respectively. These distance are in agreement with these distances reported from DFT, namely 2.31 and 2.38 Å.[26]
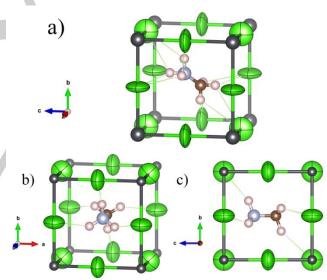
Figure 5. Schematic view of refined structures where a unique MA conformation is shown for x = 0.33 (a) and x = 1 (b) and c)). Pale-green lines illustrate the H⋯X bonds from NPD data.

Conclusions

In summary, for the first time we have found experimental evidence from diffraction data of the most likely orientation of the MA units in the perovskites of the MAPb(Br$_{1-x}$Cl$_x$)$_3$ series. The MA units in the PbX$_6$ network suffer a restriction in its dynamic disorder, where the delocalization follows the sequence: [110], [111] and [100] as the chlorine contents (x) increases from 0 to 1, and the unit cell progressively shrinks, always keeping a cubic symmetry. This sequence constitutes a clear progressive

FULL PAPER

reduction in the degrees of freedom of the MA units, considering that the delocalization along [110], [111] and [100] directions involves 6, 4 and 3 possible orientations, respectively. Furthermore, the MA orientations and their H···X distances obtained from NPD data exhibit a good agreement with the calculated values from DFT. These findings are enlightening since the crystal features obtained from NPD data can be contrasted and understood from previous results from theoretical analysis. An understanding of the structure of these compounds will assist in rationalizing how halogen-centered non-covalent interactions play an important role in the design of these materials.

Experimental Section

MAPb(Br$_{1-x}$Cl$_x$)$_3$ with x = 0, 0.33, 0.5 0.67 and 1 were obtained as microcrystalline powders from solutions of stoichiometric amounts of PbBr$_2$ (or PbCl$_2$) and MABr (or MACl) in N,N dimethyl-formamide. The choice for compositions was decided in view of the halide contents of perovskite formula, MAPbX$_3$, by replacing one (x= 0.33), two (0.66) or the three (x= 1) Br atoms per formula by Cl atoms. A particular case is x= 0.5, with Cl$_{1.5}$Br$_{1.5}$. The crystals were ground prior to the diffraction experiments. Laboratory XRD patterns were collected on a Brucker D5 diffractometer with K$_\alpha$Cu (λ = 1.5418 Å) radiation; the 2θ range was 4° up to 90° with increments of 0.03°. The NPD patterns at RT were collected in the D2B diffractometer, at the Institut Laue Langevin (ILL), Grenoble (France) with a wavelength of 1.594 Å. The use of non-deuterated samples was preferred since this is the form they will be used in devices, and the deuteration may change some structural features. The samples were contained in 6 mm diameter vanadium cylinders. NPD diffraction patterns were analysed with the Rietveld method using the *FullProf* program.[28,29] The coherent scattering lengths for Pb, Br, Cl, C, N and H were, 9.405, 6.795, 9.577, 6.646, 9.36 and -3.739 fm, respectively.

The crystal structures have been deposited via the joint CCDC/FIZ Karlsruhe deposition service, with the numbers: CCDC 1884880-1884883

[1]   G. Hodes, *Science (80-.).* **2013**, *342*, 317–318.

[2]   G. Xing, N. Mathews, S. S. Lim, N. Yantara, X. Liu, D. Sabba, M. Grätzel, S. Mhaisalkar, T. C. Sum, *Nat. Mater.* **2014**, *13*, 476–480.

[3]   Z.-K. Tan, R. S. Moghaddam, M. L. Lai, P. Docampo, R. Higler, F. Deschler, M. Price, A. Sadhanala, L. M. Pazos, D. Credgington, et al., *Nat. Nanotechnol.* **2014**, *9*, 687–692.

[4]   L. Dou, Y. Yang, J. You, Z. Hong, W.-H. Chang, G. Li, Y. Yang, *Nat. Commun.* **2014**, *5*, 5404.
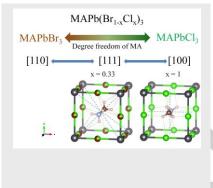
[5]   G. Maculan, A. D. Sheikh, A. L. Abdelhady, M. I. Saidaminov, M. A. Haque, B. Murali, E. Alarousu, O. F. Mohammed, T. Wu, O. M. Bakr, *J. Phys. Chem. Lett.* **2015**, *6*, 3781–3786.

[6]   J. Luo, J.-H. Im, M. T. Mayer, M. Schreier, M. K. Nazeeruddin, N.-G. Park, S. D. Tilley, H. J. Fan, M. Gratzel, *Science (80-.).* **2014**, *345*, 1593–1596.

[7]   S. Kazim, M. K. Nazeeruddin, M. Grätzel, S. Ahmad, *Angew. Chemie Int. Ed.* **2014**, *53*, 2812–2824.

[8]   C. A. López, M. V. Martínez-Huerta, M. C. Alvarez-Galván, P. Kayser, P. Gant, A. Castellanos-Gomez, M. T. Fernández-Díaz, F. Fauth, J. A. Alonso, *Inorg. Chem.* **2017**, *56*, 14214–14219.

[9]   N. Kedem, T. M. Brenner, M. Kulbak, N. Schaefer, S. Levcenko, I. Levine, D. Abou-Ras, G. Hodes, D. Cahen, *J. Phys. Chem. Lett.* **2015**, *6*, 2469–2476.

[10]   L. Wang, K. Wang, G. Xiao, Q. Zeng, B. Zou, *J. Phys. Chem. Lett.* **2016**, *7*, 5273–5279.

[11]   R. E. Wasylishen, O. Knop, J. B. Macdonald, *Solid State Commun.* **1985**, *56*, 581–582.

[12]   A. Poglitsch, D. Weber, *J. Chem. Phys.* **1987**, *87*, 6373–6378.

[13]   O. Knop, R. E. Wasylishen, M. A. White, T. S. Cameron, M. J. M. Van Oort, *Can. J. Chem.* **1990**, *68*, 412–422.

[14]   N. Onoda-Yamamuro, T. Matsuo, H. Suga, *J. Phys. Chem. Solids* **1990**, *51*, 1383–1395.

[15]   A. Maalej, Y. Abid, A. Kallel, A. Daoud, A. Lautié, F. Romain, *Solid State Commun.* **1997**, *103*, 279–284.

[16]   A. Maaej, M. Bahri, Y. Abid, N. Jaidane, Z. B. Lakhdar, A. Lautié, *Phase Transitions* **1998**, *64*, 179–190.

[17]   I. P. Swainson, R. P. Hammond, C. Soullière, O. Knop, W. Massa, *J. Solid State Chem.* **2003**, *176*, 97–104.

[18]   L. Chi, I. Swainson, L. Cranswick, J. H. Her, P. Stephens, O. Knop, *J. Solid State Chem.* **2005**, *178*, 1376–1385.

[19]   T. Baikie, N. S. Barrow, Y. Fang, P. J. Keenan, P. R. Slater, R. O. Piltz, M. Gutmann, S. G. Mhaisalkar, T. J. White, *J. Mater. Chem. A* **2015**, *3*, 9298–9307.

[20]   K. Shimamura, T. Hakamata, F. Shimojo, R. K. Kalia, A. Nakano, P. Vashishta, *J. Chem. Phys.* **2016**, *145*, 224503.

[21]   A. M. A. Leguy, A. R. Goñi, J. M. Frost, J. Skelton, F. Brivio, X. Rodríguez-Martínez, O. J. Weber, A. Pallipurath, M. I. Alonso, M. Campoy-Quiles, et al., *Phys. Chem. Chem. Phys.* **2016**, *18*, 27051–27066.

[22]   A. Varadwaj, P. R. Varadwaj, H. M. Marques, K. Yamashita, *Mater. Today Chem.* **2018**, *9*, 1–16.

[23]   X. Cheng, L. Jing, Y. Zhao, S. Du, J. Ding, T. Zhou, *J. Mater. Chem. C* **2018**, *6*, 1579–1586.

[24]   M. C. Alvarez-Galván, J. A. Alonso, C. A. López, E. López-Linares, C. Contreras, M. J. Lázaro, F. Fauth, M. V. Martínez-Huerta, *Cryst. Growth Des.* **2018**, acs.cgd.8b01463.

[25]   B. Yang, W. Ming, M.-H. Du, J. K. Keum, A. A. Puretzky, C. M. Rouleau, J. Huang, D. B. Geohegan, X. Wang, K. Xiao, *Adv. Mater.* **2018**, *30*, 1705801.

[26]   J. Li, P. Rinke, *Phys. Rev. B* **2016**, *94*, 045201.

[27]   J. M. Frost, A. Walsh, *Acc. Chem. Res.* **2016**, *49*, 528–535.

[28]   H. M. Rietveld, *J. Appl. Crystallogr.* **1969**, *2*, 65–71.

[29]   J. Rodríguez-Carvajal, *Phys. B Condens. Matter* **1993**, *192*, 55–69.

WILEY-VCH

FULL PAPER

Entry for the Table of Contents

FULL PAPER

Chloride doping in $CH_3NH_3PbBr_3$ perovskite drives a restriction in the methyl-ammonium dynamic disorder, following the sequence: [110], [111] and [100], as the unit cell progressively shrinks, always keeping a cubic symmetry.

Carlos Alberto López, *María Consuelo Álvarez-Galván, María Victoria Martínez-Huerta, María Teresa Fernández-Díaz and José Antonio Alonso**

Page No. – Page No.

Dynamic disorder restriction of methylammonium (MA) groups in chloride-doped MAPbBr₃ hybrid perovskites: a neutron powder diffraction study